PAPER

Check for updates

Binding model-tuned room-temperature phosphorescence of the bromo-naphthol derivatives based on cyclodextrins†

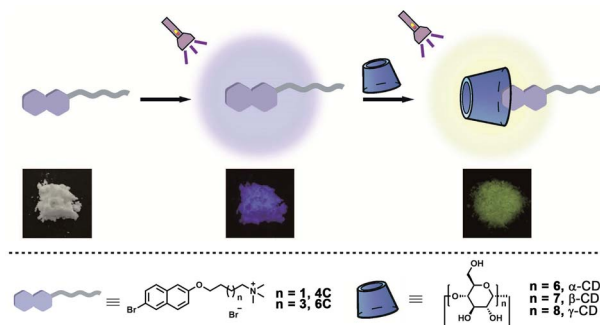Ming Liu,[a] Chen Zheng,[d] Yujing Zheng,[a] Xuan Wu[*bc] and Jianliang Shen[*abc]

Herein, bromo-naphthol derivatives were synthesized to investigate the influence on their phosphorescence emission efficiency resulting from different binding models with cyclodextrins. And the results indicated that α-cyclodextrin could result in the highest phosphorescence emission efficiency, due to the tight encapsulation of the bromo-naphthol motif into the cavity.

Organic room-temperature phosphorescence (RTP) materials have received widespread attention in the past decades owing to their potential application in anticounterfeiting,[1] biological imaging,[2,3] and optoelectronic materials.[4] However, the relatively low intersystem crossing efficiency from singlet state to the triplet state and quenching of the triplet state by external oxygen and water traditionally make it difficult to obtain the RTP materials.[5–8] Therefore, to realize the RTP materials, much effort should be devoted on the enhancement of the intersystem crossing efficiency and shielding from the oxygen and water in the environment. Along with this line, variant methods have been developed, such as polymer matrix,[9–11] crystallization,[12,13] H-aggregation,[14] and noncovalent interactions,[15–17] especially the host-guest interaction,[18–20] which could provide a relatively enclosed environment to stabilize the excited state of the organic molecules and shield them from the external substance. Even though there are many outstanding systems constructed by cucurbituril (CB)[21,22] and cyclodextrin (CD),[23,24] little research has been conducted to investigate the influence resulting from their binding model.

CD, as a kind of macrocyclic molecule, has been widely investigated in the fabrication of functional materials.[25] Moreover, due to the hydrophobic cavities in this kind of macrocyclic molecule, the phosphors could be shielded from the external environment, and many RTP systems have been successfully constructed.[26–28] However, there are three kinds of CDs with different cavity sizes, which exhibit different binding affinities to the guest molecules. To the best of our knowledge, little research has been conducted to exploit the effects caused by their binding models on the RTP materials. Herein, two bromo-naphthol derivatives (**4C** and **6C**) were synthesized to form host–guest complexation with **α-CD**, **β-CD**, and **γ-CD** (Scheme 1). Due to the different cavity size of these three host molecules, their binding models with bromo-naphthol derivatives were different, resulting in the different RTP properties. The **α-CD** could partially encapsulate the bromo-substituent motif, resulting in the highest phosphorescence quantum yield, as well as the longest phosphorescence lifetime. This research on tuning the RTP properties of phosphors by the binding models could provide a general guidance in the design of highly efficient RTP materials.

The guest molecules of **4C** and **6C** were successfully synthesized according to synthesis route provided in the ESI† (Scheme S1 and S2, ESI†). Firstly, their host–guest properties with cyclodextrins were investigated by the ^{1}H NMR spectroscopy. As shown in Fig. 1, the protons H_{1-6} of the aromatic groups in **4C** exhibited obvious shift after the addition of cyclodextrins.

[a]*School of Ophthalmology & Optometry, School of Biomedical Engineering, Wenzhou Medical University, Wenzhou, Zhejiang 32503, China. E-mail: shenjl@wiucas.ac.cn*

[b]*Wenzhou Institute, University of Chinese Academy of Sciences, Wenzhou, Zhejiang 32503, China. E-mail: wuxuan1119@ucas.ac.cn*

[c]*Oujiang Laboratory (Zhejiang Lab for Regenerative Medicine, Vision and Brain Health), Wenzhou, Zhejiang 325001, China*

[d]*College of Life and Environmental Science, Wenzhou University, Wenzhou, Zhejiang 325000, China*

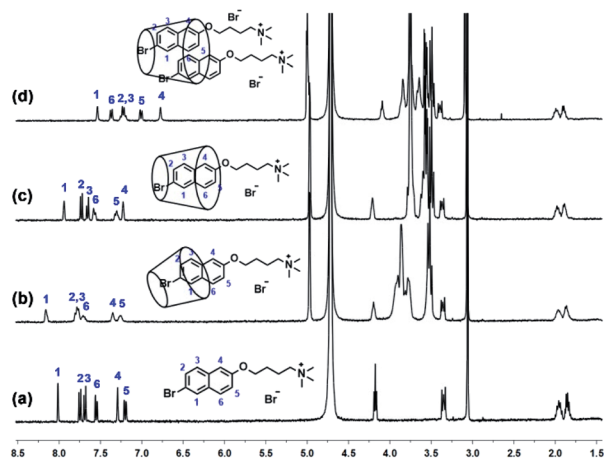Scheme 1 Schematic illustration of cyclodextrin-mediated RTP.
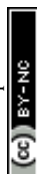
Fig. 1 ^{1}H NMR (400 MHz, D$_2$O, 298 K) spectra of **4C** (a) after adding 1.0 equivalent **α-CD** (b), **β-CD** (c), and **γ-CD** (d). ([**4C**] = [**α-CD**] = [**β-CD**] = [**γ-CD**] = 2 mM).

Interestingly, different change of the chemical-shift was observed upon the addition of **α-CD**, **β-CD**, and **γ-CD**. The protons showed downfield-shift in the presence of **α-CD** and **β-CD**, and the broaden effect could be observed in the presence of **α-CD**, which might result from the relatively small size of **α-CD**, leading to the tight encapsulation of **4C** into its cavity. And the protons exhibited the upfield-shift upon the addition of **γ-CD**, which might be caused by the $\pi \cdots \pi$ stacking interaction in the formed ternary host-guest complex. Moreover, 2D NOESY spectroscopy was employed to further investigate the binding models between **4C** and cyclodextrins. As shown in Fig. S8† in the ESI,† the corresponding peaks assigned H$_{1-3}$ on **4C** and H$_c$ on the **α-CD** were obviously observed, indicating partial aromatic ring was encapsulated into the cavity of **α-CD**. And the signals between H$_{1-6}$ on 4C and H$_c$ and H$_e$ on the **β-CD** could be observed, indicating the aromatic ring was totally encapsulated into the cavity of **β-CD** (Fig. S9, ESI†). However, the observed signals assigned to H$_{2,3,6}$ on **4C** and C$_c$ on **γ-CD** indicated the inclusion **4C** into the cavity of **γ-CD** (Fig. S10, ESI†), and the signals between H$_2$ and H$_4$ indicated the $\pi \cdots \pi$ stacking interaction between the aromatic rings. These results were consistent with the previous conclusions. Also similar phenomena could be observed in the systems of the compound **6C** and cyclodextrins with different cavity sizes (Fig. S7, ESI†). And the 2D NOESY spectra of **6C**⊂**α-CD**, **6C**⊂**β-CD**, and **6C**⊂**γ-CD** also provided the same binding models between **6C** and different cyclodextrins with cavity size.

Following, the binding stoichiometries between the **4C** and cyclodextrins were measured by Job's plot method using ^{1}H NMR spectroscopy. As shown in Fig. S14 in the ESI,† it could be concluded the 1 : 1 binding ratio was determined between **4C** and **α-CD**. Moreover, the binding stoichiometry between **4C** and **β-CD** or **γ-CD** was determined to be 1 : 1 or 2 : 1 (Fig. S15 and S16, ESI†), respectively. To determine the binding constants, titration experiments were carried out in aqueous solution containing constant concentration of **4C** (2 mM) and varying concentration of cyclodextrins respectively. And the binding

constants were calculated to be $(2.3 \pm 0.45) \times 10^3$ M^{-1} for **4C** between **α-CD** (Fig. S17, ESI†), $(2.8 \pm 0.84) \times 10^3$ M^{-1} for **4C** between **β-CD** (Fig. S18, ESI†), and $(2.7 \pm 0.39) \times 10^2$ M^{-1} and $(3.2 \pm 0.72) \times 10^3$ M^{-1} for **4C** between **γ-CD** (Fig. S19, ESI†). Also due to the main difference between **4C** and **6C** was the length of alkyl chain, the binding sites between the **6C** and cyclodextrins couldn't be affected, which was also certificated by the ^{1}H NMR and 2D NOESY spectra (Fig. S7, S11, S12, and S13, ESI†) between 6C and CDs (**α-CD**, **β-CD** and **γ-CD**), the binding stoichiometries and constants between 6C and CDs were similar with the above results.

From the above results, it could be concluded the compound **4C** could form the host–guest complexation with cyclodextrins, and due to the different size of the cavities, the binding models were different, which might result in different photoluminescence properties. Firstly, the UV-vis spectra of **4C** in the absence or presence of cyclodextrins were recorded in Fig. 2a, from which the obvious increase in the absorption intensity could be observed, indicating the formation of host–guest complexation could affect its photoluminescence properties. Moreover, the decrease of the absorption intensity at 265 and 272 nm, and the increase in the intensity at 345 nm could be observed in the presence of **γ-CD** (Fig. S20, ESI†), indicating the tightly stacking occurred between the aromatic rings of **4C**, which was consistent with the previous 2D NOSEY spectroscopy results.

Following, the host–guest complexation **4C**⊂**α-CD**, **4C**⊂**β-CD**, and **4C**⊂**γ-CD** were successfully prepared through the grinding method.[18,19] Then its photoluminescence spectra were recorded, and presented as Fig. S24 in the ESI.† From these spectra, the chromophore only emitted the blue fluorescence at 380 nm, which was consistent with the fluorescence spectrum
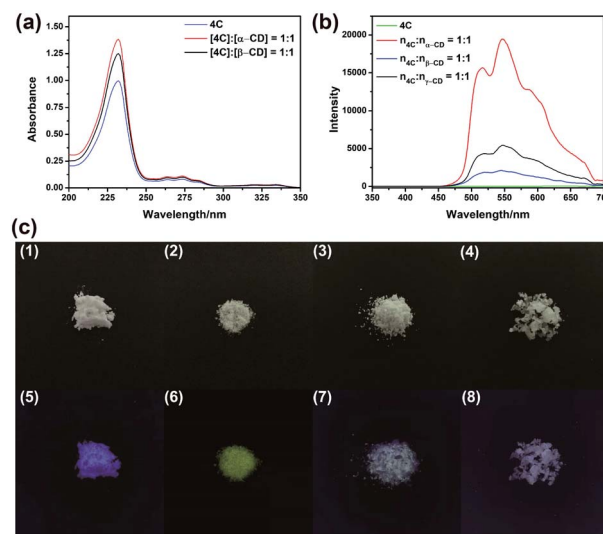

Fig. 2 (a) UV-vis spectral changes in the aqueous solution of **4C** (1.5×10^{-3} mM) upon adding equivalent **α-CD** and **β-CD**. (b) Solid state phosphorescence spectral changes of **4C**, $n_{4C}:n_{\alpha-CD} = 1 : 1$, $n_{4C}:n_{\beta-CD} = 1 : 1$ and $n_{4C}:n_{\gamma-CD} = 1 : 1$ (Ex: 280 nm, 298 K). (c)Pictures of **4C** (a and e), $n_{4C}:n_{\alpha-CD} = 1 : 1$ (b and f), $n_{4C}:n_{\beta-CD} = 1 : 1$ (c and g) and $n_{4C}:n_{\gamma-CD} = 1 : 1$ (d and h) under ambient light (a–d) and 365 nm lamp (e–h).

in the aqueous solution (Fig. S21, ESI†). This result also further certificated by the determination of its luminescence lifetime, from the decay curve, its lifetime was determined to be 0.77 ns. However, the addition of cyclodextrins could result in the appearance of the new emission peaks at 518 nm and 548 nm, and the average lifetimes at both 518 nm and 548 nm remarkably improved, indicating the formation of host–guest complexation could stabilize the triplet of **4C** (Table 1 and S3, ESI†). This observation was also consistent with the photographs obtained under the UV light irradiation (365 nm). As shown in Fig. 2c, the solid of **4C** emitted the violet luminescence, and the yellow luminescence could be observed from **4C⊂α-CD**. However, the yellow luminescence was remarkably reduced in the complexation of **4C⊂β-CD**, and **4C⊂γ-CD**. This observation was also consistent with the previous results, the addition of **α-CD** could remarkably improve the phosphorescence intensity. Moreover, their quantum yields of luminescence were further determined. As being presented in Table 1, the absolute fluorescence and phosphorescence quantum yields of **4C** were determined to be 0.29% and 0.56%, respectively. After being formation of host–guest complexation, the fluorescence quantum yields increased, along with the increase in the phosphorescence quantum yields (Table 1). And the **4C⊂α-CD** exhibited the highest phosphorescence quantum yields, whose value was increased to 11.47%.

Interestingly, the similar phenomena could also be observed in the systems constructed by **6C** (Fig. S25, S26, S32, and Table S1, S3, ESI†). Therefore, a conclusion might be drawn that the cyclodextrins could improve the phosphorescence quantum yield, as well as prolong the decay time of phosphorescence. As is well known, the phosphor should exhibit more intensive photoluminescence in a more restricted circumstance, in these systems, the addition of cyclodextrins would encapsulate the phosphor into the cavity of the macrocyclic molecules. Moreover, different cyclodextrins exhibited different efficiency in the promotion of its photoluminescence properties. From the previous results obtained from the 2D NOESY spectroscopy, the partial aromatic rings containing the bromo unit was encapsulated into the cavity of **α-CD**, in this manner, the rotation of the guest molecule might be restricted, as well as the bromine atom was shielded from the outer environment, which would enhance the ISC and suppress the nonradiative relaxation, resulting in the promotion in the quantum yield and the prolongation of the lifetime. And in the host–guest complexation of **4C⊂β-CD**, the entire aromatic ring was encapsulated into the cavity of **β-CD** due to the relatively larger cavity compared with **α-CD**. However, there would be more space for the rotation in the cavity, which could increase the nonradiative

relaxation. This phenomenon also accounted for the relative lower quantum yield and lifetime of **4C⊂β-CD**. And in the **4C⊂γ-CD**, the π···π stacking was occurred in the cavity of the γ-CD, resulting in the further astrictions of the rotation of **4C** even though in the largest cavity of cyclodextrins.

To further confirm the host–guest interaction played a vital role in the promotion of quantum yields of phosphorescence. Compound **4C** was employed as the model compound for the following experiments. The glucose (glu) was used as the model compound due to its being the repeating unit of the cyclodextrins. By using the same grinding method, the mixture of **4C@Glu** was obtained. And from the obtained spectra (Fig. 3b), it was observed the addition of glucose could not remarkably improve the phosphorescence emission of **4C**, which might result from the absence of the hydrophobic cavity to encapsulate the phosphors. Then the molar ratio of **a-CD** and **4C** was further increased to certificate our envision. The obtained results were consistent with our anticipation, with the increase in the **α-CD** content, the phosphorescence emission intensity was enhanced. And the following determination of their phosphorescence quantum yields also further certificated the above results. And with the increase in the **α-CD** content, the quantum yield was increased from 11.47% to 20.24%, which might be caused by the incomplete complexation at the lower content of the **α-CD**. And the photographs of the solid under the UV light also provided the same results, in which the solid with the highest molar ratio between cyclodextrin and 4C presented the brightest yellow lights (Fig. S31, ESI†). These phenomena also indicated the cavity of cyclodextrin played a vital role in improving its phosphorescence emission.

To confirm the formation of host–guest complexation in the solid state, the Fourier transform infrared (FTIR) spectroscopy was employed. As shown in Fig. S33 in the ESI†, the peak assigned to C–H stretching vibration at 3003 cm^{-1}, 2945 cm^{-1},
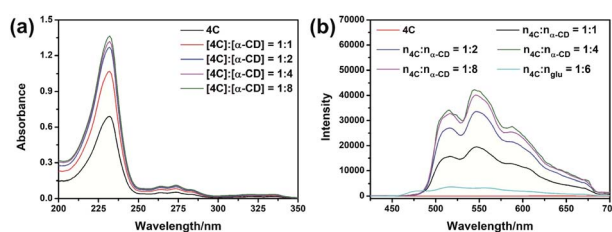

Fig. 3 (a) UV-vis spectral changes in the aqueous solution of **4C** (1.5×10^{-3} mM) upon adding different equivalent **α-CD**. (b) Solid state phosphorescence spectral changes of **4C**, $n_{4C}:n_{\alpha-CD} = 1:1$, $n_{4C}:n_{\alpha-CD} = 1:2$, $n_{4C}:n_{\alpha-CD} = 1:4$, $n_{4C}:n_{\alpha-CD} = 1:8$, $n_{4C}:n_{glu} = 1:6$ (Ex: 280 nm, 298 K).

Table 1 The photophysical data of **4C**, **4C⊂α-CD**, **4C⊂β-CD**, and **4C⊂γ-CD** in the solid state (Ex: 280 nm, 298 K)

	τ_{Phos} at 548 nm ms^{-1}	τ_{Phos} at 518 nm ms^{-1}	τ_{Fluo} at 380 nm ns^{-1}	Φ_{phos}/%	Φ_{fluo}/%
4C	0.48	0.78	0.77	0.56	0.29
$n_{4C}:n_{\alpha-CD} = 1:1$	5.89	6.92	3.46	11.47	0.49
$n_{4C}:n_{\beta-CD} = 1:1$	6.03	6.00	1.87	3.07	0.98
$n_{4C}:n_{\gamma-CD} = 1:1$	3.94	3.97	1.32	5.73	0.58

and 2867 cm^{-1} could be obviously observed. Upon the addition of **α-CD**, these peaks broadened, and shifted to 2983 cm^{-1} and 2916 cm^{-1}. This might be resulted from the formation inclusion complex between **4C** and **α-CD**, which could decrease the distance between the C–H bond on the aromatic ring and the O atoms in the **α-CD**, resulting in the enhanced hydrogen bond interaction. Moreover, the XRD was also carried out to certificate the host–guest interaction in the solid state. From the obtained spectra (Fig. S34, ESI†), the scattering signals of **4C** changed upon the addition of **α-CD**, indicating the addition of **α-CD** could change the pattern model of **4C**. Moreover, the distance of the aromatic rings was changed from 6.20 Å ($2\theta = 14.28°$) to 6.75 Å ($2\theta = 13.10°$) in the presence of **α-CD**. These results presented a solid evidence for the formation of host–guest complexation in the solid state.

Herein, two bromo-naphthol derivatives were synthesized to form host–guest complexation with **α-CD**, **β-CD**, and **γ-CD**. Even though the binding affinities between the bromo-naphthol derivative and CDs were similar, their RTP efficiency was different. The host–guest complexation formed with **α-CD** presented the highest phosphorescence quantum yield, as well as the longest phosphorescence lifetime. In this complexation, the bromo-substituent motif was encapsulated into the cavity, therefore the exciting state could be stabilized, and shielded form the external environment, resulting in the enhancement in the RTP emission. This research on tuning the RTP properties of phosphors by the binding models could provide a general guidance in the design of highly efficient RTP materials.

Conflicts of interest

There are no conflicts to declare.

References

1 J. Tan, Q. Li, S. Meng, Y. Li, J. Yang, Y. Ye, Z. Tang, S. Qu and X. Ren, *Adv. Mater.*, 2021, **33**, 2006781.
2 Q. Dang, Y. Jiang, J. Wang, J. Wang, Q. Zhang, M. Zhang, S. Luo, Y. Xie, K. Pu, Q. Li and Z. Li, *Adv. Mater.*, 2020, **32**, 2006752.
3 Y. Wang, H. Gao, J. Yang, M. Fang, D. Ding, B. Z. Tang and Z. Li, *Adv. Mater.*, 2021, **33**, 2007811.
4 C.-J. Zheng, C.-L. Liu, K. Wang, S.-L. Tao, H. Lin and C.-S. Lee, *Sci. China: Chem.*, 2017, **60**, 504–509.
5 A. D. Nidhankar, Goudappagouda, V. C. Wakchaure and S. S. Babu, *Chem. Sci.*, 2021, **12**, 4216–4236.
6 X. Yan, H. Peng, Y. Xiang, J. Wang, L. Yu, Y. Tao, H. Li, W. Huang and R. Chen, *Small*, 2022, **18**, 2104073.
7 H. Shen, C.-A. Di and D. Zhu, *Sci. China: Chem.*, 2017, **60**, 437–449.

8 Y. Liu, G. Zhan, Z.-W. Liu, Z.-Q. Bian and C.-H. Huang, *Chin. Chem. Lett.*, 2016, **27**, 1231–1240.
9 X. Chen, C. Xu, T. Wang, C. Zhou, J. Du, Z. Wang, H. Xu, T. Xie, G. Bi, J. Jiang, X. Zhang, J. N. Demas, C. O. Trindle, Y. Luo and G. Zhang, *Angew. Chem., Int. Ed.*, 2016, **55**, 9872–9876.
10 H. Wang, H. Shi, W. Ye, X. Yao, Q. Wang, C. Dong, W. Jia, H. Ma, S. Cai, K. Huang, L. Fu, Y. Zhang, J. Zhi, L. Gu, Y. Zhao, Z. An and W. Huang, *Angew. Chem., Int. Ed.*, 2019, **58**, 18776–18782.
11 G. Wang, Z. Wang, B. Ding and X. Ma, *Chin. Chem. Lett.*, 2021, **32**, 3039–3042.
12 O. Bolton, K. Lee, H.-J. Kim, K. Y. Lin and J. Kim, *Nat. Chem.*, 2011, **3**, 205–210.
13 Q. Xiong, C. Xu, N. Jiao, X. Ma, Y. Zhang and S. Zhang, *Chin. Chem. Lett.*, 2019, **30**, 1387–1389.
14 L. Bian, H. Shi, X. Wang, K. Ling, H. Ma, M. Li, Z. Cheng, C. Ma, S. Cai, Q. Wu, N. Gan, X. Xu, Z. An and W. Huang, *J. Am. Chem. Soc.*, 2018, **140**, 10734–10739.
15 O. Bolton, D. Lee, J. Jung and J. Kim, *Chem. Mater.*, 2014, **26**, 6644–6649.
16 S. Hirata, K. Totani, J. Zhang, T. Yamashita, H. Kaji, S. R. Marder, T. Watanabe and C. Adachi, *Adv. Funct. Mater.*, 2013, **23**, 3386–3397.
17 Z. Wang, T. Li, B. Ding and X. Ma, *Chin. Chem. Lett.*, 2020, **31**, 2929–2932.
18 Z.-Y. Zhang and Y. Liu, *Chem. Sci.*, 2019, **10**, 7773–7778.
19 Z.-Y. Zhang, W.-W. Xu, W.-S. Xu, J. Niu, X.-H. Sun and Y. Liu, *Angew. Chem., Int. Ed.*, 2020, **59**, 18748–18754.
20 G. Qu, Y. Zhang and X. Ma, *Chin. Chem. Lett.*, 2019, **30**, 1809–1814.
21 D.-A. Xu, Q.-Y. Zhou, X. Dai, X.-K. Ma, Y.-M. Zhang, X. Xu and Y. Liu, *Chin. Chem. Lett.*, 2022, **33**, 851–854.
22 J. Wang, Z. Huang, X. Ma and H. Tian, *Angew. Chem., Int. Ed.*, 2020, **59**, 9928–9933.
23 D. Li, F. Lu, J. Wang, W. Hu, X.-M. Cao, X. Ma and H. Tian, *J. Am. Chem. Soc.*, 2018, **140**, 1916–1923.
24 X. Lin, Q. Xu and X. Ma, *Adv. Opt. Mater.*, 2022, **10**, 2101646.
25 Y.-M. Zhang, Y.-H. Liu and Y. Liu, *Adv. Mater.*, 2020, **32**, 1806158.
26 G. Huang, Z. Deng, J. Pang, J. Li, S. Ni, J.-A. Li, C. Zhou, H. Li, B. Xu, L. Dang and M.-D. Li, *Adv. Opt. Mater.*, 2021, **9**, 2101337.
27 H. Chen, L. Xu, X. Ma and H. Tian, *Poly. Chem.*, 2016, **7**, 3989–3992.
28 J.-J. Li, H.-Y. Zhang, Y. Zhang, W.-L. Zhou and Y. Liu, *Adv. Opt. Mater.*, 2019, **7**, 1900589.